November 14, 2007

Compact Microfluidic Structures for Generating Spatial and Temporal Gradients

Dragos Amarie, *Georgia Southern University*
James A. Glazier, *Indiana University - Bloomington*
Stephen C. Jacobson, *Indiana University - Bloomington*

Published in final edited form as:
Anal Chem. 2007 December 15; 79(24): 9471–9477. doi:10.1021/ac0714967.

Compact Microfluidic Structures for Generating Spatial and Temporal Gradients

Dragos Amarie[†,‡,§], **James A. Glazier**[‡,§], and **Stephen C. Jacobson**[*,†]
Department of Chemistry, Department of Physics, and Biocomplexity Institute, Indiana University, Bloomington, Indiana 47405-7102

Abstract

We present an improved microfluidic design for generating spatial and temporal gradients. The basic functional elements are bifurcated and trifurcated channels used to split flow between two and three channels, respectively. We use bifurcated channels on the exterior of the channel manifold and trifurcated channels in the interior with mixing tees to recombine flows. For N gradient-forming levels, the number of discrete steps in the gradient is $2^N + 1$, allowing a compact gradient-forming structure that is only 1.6 mm long and 0.5 mm wide. Control of the relative sample concentration at the inlets enables generation of gradients with varying slopes and offsets. The small total channel length allows faster switching (only 2.6 s) between gradients of different compositions than did previous designs, allowing complex temporal sequences and reducing total displacement volume and reagent use. The design permits opposing-gradient experiments and generation of complex nonlinear gradients. We fabricated and tested three channel designs with either three or four gradient-forming levels, 20- or 40-μm channel widths, 60-or 120-μm center-to-center channel spacings, and 9 or 17 output steps. These devices produced essentially identical high-quality linear gradients using both pressure-driven and electrokinetic flow.

Over the past 15 years, microfluidic devices have enabled miniaturized chemical and biochemical analysis applications, known as lab-on-a-chip technologies.[1] The small lateral dimensions of microfluidic channels, typically 1–100 μm, permit precise manipulation of nanoliter to attoliter fluid volumes using applied hydrostatic forces, voltages, or both. Microfluidic devices permit temporally and spatially precise and reproducible fluid delivery.

Chemical concentrations varying in time or space are of particular interest for drug discovery, medical diagnostics, and biomedical research applications. To create temporal gradients, we typically mix fluids in different ratios at a channel junction by varying the applied potentials or pressures with time.[2] These gradients find use in enzyme assays[3] and chromatographic separations.[4,5] To form spatial gradients, we disperse the chemical of interest laterally across one or more microchannels. The gradient-forming region (also called a gradient ladder or gradient-forming network) typically lies between two or more input reservoirs and a gradient chamber and uses multiple mixing levels or controlled mixing ratios to generate gradients with different shapes. Early designs include series of cross intersections, which serially diluted the sample;[6] arrays of mixing tees with different channel lengths, which divided the sample at different ratios;[6] and multilevel pyramidal structures, which split and recombined flows.[7,8] The pyramidal design also permitted temporal control of gradients.[9] A more recent design positions flow dividers in different patterns within a microchannel to produce gradients for a

* Corresponding author. E-mail: jacobson@indiana.edu.
† Department of Chemistry.
‡ Department of Physics.
§ Biocomplexity Institute.

variety of functions.[10] Other methods create flow-free gradients by coupling microchannels to agarose gels[11] or porous membranes;[12] flow-free gradients are beneficial where flow may influence cell movement.

Current gradient-based biological assays use capillaries;[13,14] Boyden,[15] Zigmond,[16] or Dunn chambers;[17] or pyramidal micro-fluidic ladders to produce concentration gradients. Biological assays include chemotaxis assessment of neutrophils,[18] hippocampal neurons,[19] leukemia cells expressing a transfected chemokine receptor,[20] and *Escherichia coli*.[12] Simpler designs use three input channels to measure chemotaxis in *E. coli*[21] and mouse sperm cells[22] and Y-shaped channels to assay T-cell chemotaxis.[23] One recent example employs microfluidics to generate chemical gradients over 5 orders of magnitude in concentration.[24]

The key needs for gradient generation include small sample and displacement volumes to minimize reagent usage and permit rapid temporal changes in gradients, small total device size to allow multiple gradient chambers per chip for high-throughput applications, and high temporal and spatial stability of gradients. The ability to generate spatially and temporally complex gradients and to independently manipulate multiple or opposing gradients is also useful in some applications.

Different gradient-generation approaches have different combinations of advantages and disadvantages. In general, microfluidic methods are smaller and better on all counts than their macroscopic T (Y)-type or H-type forebears, which could produce flow-free gradients but had poor stability, quantitative accuracy, and temporal response; permitted only sigmoidal spatial profiles; and could not produce complex temporal profiles. Among microfluidic designs, pyramidal gradient-forming networks have large displacement volumes compared to T- or H-type designs and have fairly slow response, but can produce arbitrary temporal and spatial gradients and have excellent accuracy and stability. Their main defect is that they require combination with permeable membranes to produce flow-free gradients. Pyramidal designs provide a fixed number of output channels at different dilutions to the sample chamber. More channels produce a smoother, more stable gradient but increase the size of the ladder circuitry and slow temporal response.

Our design keeps some features of the pyramidal-ladder geometry, while reducing device size and displacement volume by a factor of 10, which also improves temporal response. The device uses bifurcated and trifurcated channels for mixing, reducing the number of mixing levels needed for a given number of output channels. Using trifurcated channels proved critical to reducing the number of layers required to form gradients because each trifurcation not only passes the input sample concentration to the next level but also splits the input sample to be mixed with both higher and lower concentrations of sample at adjacent mixing tees. For example, to form a gradient network with nine output channels from two input reservoirs, our design requires three levels of dividers, while the pyramidal design requires seven. In general, for N divider layers, our design produces $2^N + 1$ outputs, while the pyramidal design produces $N + 2$ outputs. The reduced number of levels simplifies device design and greatly reduces device footprint. Adjusting the input concentrations to the gradient-forming region permits gradients with variable slopes and adjustable offsets. The compact design and narrow channels reduce latency to less than 2.6 s.

EXPERIMENTAL SECTION

Master Fabrication

We formed the masters on glass substrates (75 × 50 × 1 mm) cleaned in HCl/HNO_3 (3:1), rinsed with water (18 MΩ·cm, Super-Q Plus, Millipore Corp.), dried with nitrogen, sonicated in methanol and acetone (1:1), and dried with nitrogen. The master had two SU-8 2010

(MicroChem Corp.) photoresist layers, where the first layer (~20 μm thick) promoted adhesion of the channel structure to the substrate, and the second layer (~20 μm thick) became the channel structure. Processing of both layers was identical, except the first layer exposure did not use a photomask. We spin-coated (PWM32-PS-R790, Headway Research, Inc.) the photoresist on the substrate by ramping at 40 rpm/s to 1000 rpm and holding at 1000 rpm for 30 s. Prior to exposure, we baked the photoresist on a digital hot plate (732P, PMC Industries) at 65 °C for 1 min, ramped to 95 °C at 100 °C/h, and held at 95 °C for 3 min. Photomask design used AutoCAD LT 2004 (AutoDesk, Inc.). We had the design printed on a transparency using a high-resolution laser photoplotter at 40 640 dpi (Photoplot Store) and contact-printed the design on the photoresist using a UV exposure system (205S, Optical Associates, Inc.) equipped with a high-pressure Hg arc lamp and an additional 360-nm band filter (fwhm 45 nm, Edmund Optics, Inc.) with a total exposure of 300 mJ/cm^2. We postbaked the exposed photoresist on the hot plate maintained at 65 °C for 1 min, ramped to 95 °C at 300 °C/h, and held at 95 °C for 1 min and then developed the master for 10 min, rinsed with 2-propanol, and dried with nitrogen. The channel height of the SU-8 master was 19.2 ± 0.1 μm averaged over 10 measurements across the master with a stylus profiler (Dektak 6M, Veeco Instruments, Inc.).

Channel Fabrication

We cast microchannels in poly(di-methylsiloxane) (PDMS) substrates using the SU-8 masters.[25,26] The silicone elastomer kit (Sylgard 184, Dow Corning Corp.) contains a polymer base and curing agent, which were mixed in a 10:1 ratio for 2–3 min. A tape barrier around the master held the elastomer mixture in place as it was poured onto the master. We placed the PDMS on the master under low vacuum (~1 Torr) for 1 h to enhance channel replication, then cured the PDMS at 100 °C for 30 min, and immediately separated the hot PDMS substrate from the master, avoiding the need for silanization of the master. Access holes punched through the elastomer to the channels with a 16-gauge needle or a 3-mm cork borer provided fluid access for pressure-driven or electrokinetic flow, respectively.

Chip Assembly

The cleaning sequence for the PDMS substrates was to rinse with methanol, rinse with toluene for less than 1 min, and sonicate for 3 min in methanol to remove residual toluene and any surface debris. The cleaning sequence for the glass cover plates included exposure to NH_4OH/H_2O_2/H_2O (2:1: 1) for 1 h at 75 °C, a water rinse, and a nitrogen dry. We exposed both the PDMS substrate and glass cover plate to an air plasma (PDC-32G, Harrick Plasma) for 40 s and joined them permanently. Priming the microfluidic channels with buffer (10 mM sodium tetraborate) through the waste reservoir minimized bubble formation and uniformly wet the channels.

Optical Imaging

We imaged fluid gradients using an inverted optical microscope (TE2000-U, Nikon, Inc.) equipped with a high-pressure Hg arc lamp and a CCD camera (CoolSnap HQ or Cascade 512B, Photometrics) controlled using MetaMorph imaging software (Molecular Devices Corp.). We placed a 100 μM solution of disodium fluorescein in 10 mM sodium tetraborate buffer in inlets 1a and 2a as a fluorescent probe and borate buffer without fluorescein in inlets 1b and 2b, allowing relative fluorescein concentrations from 0 to 100% at tees 1 and 2 (see Figure 1). To process line profiles from the images, we averaged four rows of pixels for each line profile, subtracted a background line profile, and normalized to a line profile of the gradient chamber filled entirely with the fluorescein solution. The processed line profiles corresponded to a 2.58-μm wide region in the vertical direction of the gradient chamber.

Flow Control

We used both pressure-driven and electrokinetic flow to form gradients. For the pressure-driven flow, we connected the ends of each channel on the microchip to separate 10-mL graduated cylinders (mounted on vertical positioning stages) using 1.6-mm-o.d. polypropylene tubing.[22] Fluorescent polystyrene beads (770-nm diameter, PolySciences, Inc.) added to the buffer in the inlet reservoirs (10^4 beads/μL) served as velocity tracers to permit measurement of the flow rates within the channels. We defined the reference cylinder level when the fluid heights in the inputs and waste cylinders were level, and we observed no fluid flow in the channels. Adjusting the relative heights (ΔH) of the graduated cylinders with respect to the reference level controlled the hydrostatic pressure. Lowering the waste reservoir to $\Delta H_{waste} = -8.5$ mm produced a 100 μm/s flow in the gradient chamber. Under this condition, the fluorescein concentration within the gradient chamber was uniform (no gradient), i.e., 50% from inlet 1 and 50% from inlet 2. Adjusting the cylinder heights for inlet 1a relative to inlet 1b for mixing tee 1 and inlet 2a relative to inlet 2b for mixing tee 2 controlled the relative fluorescein concentrations at mixing tees 1 and 2 (0–100%) hydrostatically. Adjustment of the cylinder heights was simultaneous, in opposite directions, and of the same displacement with respect to the reference level. For example, setting the cylinders connected to inlets 1a and 1b to $\Delta H_{1a} = 2.2$ mm and $\Delta H_{1b} = -2.2$ mm produced a 75% fluorescein level at mixing tee 1.

Electrical potentials applied to the inlet reservoirs using custom-built high-voltage power supplies, controlled using Lab-View (National Instruments Corp.), enabled electrokinetic transport. Syringe filters (0.22-μm pore size) inserted into the channel access holes in the PDMS layer and filled with buffer served as reservoirs. Pt electrodes inserted in the syringe filters provided electrical contact to the buffer. We defined the reference voltage ($V_{ref} = 200$ V) to be when the fluorescein velocity in the gradient chamber was 100 μm/s, and the flow from inlets 1 and 2 were balanced (no gradient), i.e., 50% from inlet 1 and 50% from inlet 2. Adjusting the potentials applied to inlet 1a relative to inlet 1b for tee 1 and to inlet 2a relative to inlet 2b for tee 2 ($\Delta V_{inlet} = 0$–90 V) controlled the relative fluorescein concentrations at tees 1 and 2 (0–100%). Changes to the applied potentials were simultaneous, of opposite sign and of the same magnitude with respect to the reference voltage. For example, setting the potentials at inlets 1a and 1b to $\Delta V_{1a} = 60$ V and $\Delta V_{1b} = -60$ V with respect to the reference voltage produced a 75% fluorescein level at tee 1. The experiments with electrokinetic flow used microfluidic devices bonded earlier the same day, and we observed no change in the electrokinetic flow over the course of the experiments.

RESULTS AND DISCUSSION

Microfluidic Device Design

Figure 1 shows a schematic of a three-level gradient-forming network. The three primary components of the structure are the inlets, gradient-forming region, and gradient chamber. The section above about flow control describes how inlets 1 and 2 can deliver the sample to mixing tees 1 and 2 at any concentration between 0 and 100%. Concentrations 1 and 2 from mixing tees 1 and 2, respectively, flow through the gradient-forming region and exit into the top of the gradient chamber, allowing linear gradients with positive or negative slopes, and any offset or concentration between 0 and 100%.

Figure 2a shows the design of the gradient-forming network. Our basic principle is to mix concentrations 1 and 2 from mixing tees 1 and 2 both in parallel and in series by repetitively splitting and merging streams, while maintaining concentration 1 down the left side of the device and concentration 2 down the right side. For N gradient-forming levels, the number of discrete steps (n) forming the chemical gradient, which equals the number of output channels, is

$$n=2^N+1 \quad (1)$$

The difference in concentration, C_{step}, between adjacent output channels at level N is

$$C_{step}=\frac{|C_1 - C_2|}{2^N} \quad (2)$$

where C_1 and C_2 are concentrations 1 and 2, respectively. For example, one level produces concentrations separated by 50%, two levels by 25%, three levels by 12.5%, and four levels by 6.25%.

We designed the gradient-forming network in stages, starting from the gradient chamber and working our way back to the input channels, according to two criteria: (1) the flow velocity from each channel entering the gradient chamber must be the same, and (2) the pressure or potential drop across any gradient-forming level must be constant. Each level consists of transfer channels and connector channels (see Figure 2a). Within a level, the transfer channels are the same length, and the variable-length connector channels combine flows and adjust the flow resistance. $T_{L,i}$ denotes a transfer channel, where L is the level index (1 to N) and i is the transfer channel number from left to right. We choose the transfer-channel length to allow a sample entering a mixing tee (Figure 2d) sufficient time to mix by diffusion,

$$\sigma=\sqrt{2Dt}=\sqrt{2D\frac{l}{u}} \quad (3)$$

where σ is the distance a soluble component diffuses in time t, D is the diffusion coefficient of the component, l is the channel length, and u is the velocity. In our case, we assumed complete mixing when σ reached half the channel width w. Similarly, $C_{L,j}$ denotes a connector channel, where L is the level index and j is the connector channel number from left to right. We adjust the connector-channel lengths, which control the hydrodynamic resistance, to maintain a constant hydrostatic potential drop across a level for all flow paths. As a result, the exterior channels in Figures 2a and 3a are longer than the interior channels.

As in traditional pyramidal-ladder designs, the output into the gradient chamber is a series of step concentrations ranging from concentration 1 (from mixing tee 1) to concentration 2 (from mixing tee 2). Within the chamber, diffusion smoothes the profile proceeding in the direction of flow. The more output steps, the smoother the gradient, the shorter the flow length to smoothness, and the greater the accuracy and stability of the gradient.

To calculate the concentration at each point in the gradient chamber, we describe the concentration due to each stream carrying a nonzero concentration in a one-dimensional concentration space as an appropriate error function (erf). The resulting normalized concentration profile $C(x,l)/C_0$ is a sum of these erfs,[27]

$$\frac{C(x,l)}{C_0}=\frac{1}{2}\left[1+\frac{1}{n-1}\sum_{i=1}^{n-1}\mathrm{erf}\left(\frac{i-r(x)}{a(l)}\right)\right] \quad (4)$$

where x is the lateral position in the gradient chamber, $r = x/s$ is the normalized lateral position, l is the position along the direction of flow, $a = (2^{1/2})\sigma/s = (4Dt)^{1/2}/s = (4Dl/u)^{1/2}/s$ is the normalized diffusive width of a single stream, $C_0 = |C_1 - C_2|$ is the concentration difference between inlets 1 and 2, s is the center-to-center spacing between adjacent input streams, u is the mean flow velocity, and n is the total number of outputs into the gradient chamber.

The three basic structures in the gradient-forming network are bifurcated channels (Figure 2b), trifurcated channels (Figure 2c), and mixing tees (Figure 2d). A bifurcated channel splits the input flow (in1) into two output streams (out1, out2) and connects exterior channels. A trifurcated channel divides the input flow (in3) into three output streams (two out2, out3) and connects interior channels. A mixing tee combines two input flows (in2) into a single output (out3) with the inputs coming from either the bi- or trifurcated channels (out2). The combined streams must flow sufficiently slowly that they mix by diffusion before reaching the next level or the gradient chamber.

The input and output flow velocities for any gradient-forming level depend on the total number of levels of the design (N), the level index (L), and the flow velocity (u_f) in the final level's (f) output channels as they enter the gradient chamber. In Figure 2b–d, the input and output velocities for the bifurcated, trifurcated, and mixing channels are

$$u_{in1}(N,L)=u_{out1}(N,L)=(2^{N-L-1}+(1/2))u_f \quad (5)$$

$$u_{in2}(N,L)=u_{out2}(N,L)=2^{N-L-1}u_f \quad (6)$$

$$u_{in3}(N,L)=u_{out3}(N,L)=2^{N-L}u_f \quad (7)$$

where the level index (L) increases at output bifurcation intersections only, not in the middle of channels or at the input bifurcations (see Figure 2). For example, channel in3 feeds channel out3 in the next gradient-forming level, but channel out3 feeds channel in3 in the same level.

Gradient Formation

We fabricated and tested three different gradient-forming designs with different numbers of gradient-forming levels (three or four), channel widths (20 or 40 μm), and center-to-center output-channel spacings (60 or 120 μm). The names of the devices 3-20-60, 3-40-120, and 4-20-60 correspond to their number of levels, channel widths, and channel spacings, respectively. Table 1 summarizes their dimensions. The gradient- chamber width is the number of output channels times their center-to-center spacing. The gradient chamber ended in a tapered region connecting to a channel that flows into a waste reservoir.

Our design assumes a liquid flow velocity of 100 μm/s in the gradient chamber, which is typical in microfluidic chemotaxis assays.[18] For each chip, we measured the gradient profile at a longitudinal position l corresponding to a = 0.745 (eq 4). This value corresponds to l = 100 μm for devices 3-20-60 and 4-20-60 and l = 400 μm for device 3-40-120. At these positions, using $D = 5 \times 10^{-6}$ cm^2/s for fluorescein,[28] eq 4 predicts a maximum deviation of 0.02% from an ideal linear gradient. In our experiments, the gradients deviated less than 1% from the expected linear shape. The average flow velocity for 50 beads (770-nm diameter) was 99.8 ± 7.4 μm/s for pressure-driven flow and 96.8 μm/s for electrokinetic flow, estimated by timing the displacement of the fluorescein front along the flow direction. These velocities were stable for up to 20 h.

The fluorescence images in Figures 3 and 4 depict the gradient formed using device 3-20-60 in the gradient-forming region and gradient chamber, respectively. Figure 3b shows 100% concentration 1 from mixing tee 1 mixing with 0% concentration 2 from mixing tee 2, and Figure 3c shows the mirror image. The images in Figure 3 show that the sample and buffer mixed completely in the transfer channels in each layer before reaching the next layer in the gradient forming region, and Figure 4 depicts how the gradients extended down the chamber. Figure 5a shows gradients with varying slopes for concentration 2 at mixing tee 2 set to 0% and varying concentration 1 at mixing tee 1 from 100 to 25% in 25% steps (Figure 5a profiles

1a–1d), and for concentration 1 set to 0% and varying concentration 2 from 100 to 25% in 25% steps (Figure 5a profiles 2a–2d). We also produced gradients with variable offsets and constant slope. Figure 5b shows a series of gradient profiles with ΔC = 25% across the gradient chamber and offsets in 25% increments. In Figure 5b**,** profiles 1e–1h have concentration 1 stepped from 100 to 25% in 25% increments with concentration 2 simultaneously stepped from 75 to 0% also in 25% increments. In Figure 5b**,** profiles 2e–2h show the mirror images, switching relative concentrations 1 and 2. When changing the gradient composition, we typically adjusted the cylinder heights, waited for 10 s, and imaged the new composition. The time to achieve a new stable gradient was 2.6 s for device 3-20-60, which corresponded to displacing 5.27 nL in the gradient-forming region between tees 1 and 2 and the gradient chamber. For comparison, the volume of the gradient-forming region of the pyramidal design[8] is ~0.84 μL, and the changeover time to replace the fluid between the mixing tees and the gradient chamber is 18 s at the reported linear velocity of 1 mm/s and 180 s at a linear velocity of 0.1 mm/s.

In order to evaluate the effects of the number of gradient-forming levels and of the channel spacing, we compared gradients formed using devices 3-20-60, 3-40-120, and 4-20-60. Figure 6 shows the gradient-forming regions for devices 3-40-120 and 4-20-60 at the same magnification. The exterior channels and level lengths differ due to the need to balance flows and maintain sufficient in-channel diffusion. Figure 7 shows gradients for concentration 1 at 100% and concentration 2 at 0% for l = 100 μm for devices 3-20-60 and 4-20-60 and l = 400 μm for device 3-40-120. The extra level in device 4-20-60 produces 6.25% concentration steps rather than 12.5% steps for the other devices, yielding a larger linear region, covering 94% of the width of the gradient chamber compared to 88% for the other devices. However, Figure 7 shows that the additional level did not substantially improve the linearity of the gradient, for which the average difference between the experimental and theoretical gradient profiles was <1%. Similarly, the increase in channel spacing from 60 to 120 μm between devices 3-20-60 and 3-40-120 produced linear gradients, although the gradient took four times longer to reach linearity due to the increase in channel spacing. To quantify the difference between the theoretical and experimental profiles, we subtracted the theoretical gradient profiles from the experimental gradient profiles and calculated the standard deviation between the two. The relative standard deviations between the experimental and theoretical gradients were 0.8, 0.9, and 0.4% for devices 3-20-60, 3-40-120, and 4-20-60, respectively, meeting our criterion for a linear gradient, i.e., < 1% difference between the theoretical and experimental gradient profiles.

Figures 3–5 and 7 show gradients generated with pressure-driven flow. To compare gradients produced with pressure-driven (Figure 8a) and electrokinetic (Figure 8b) flows, we set concentration 2 to 50% and varied concentration 1 from 100 to 0% in 25% increments (Figure 8a profiles 1i–1m for pressure-driven flow and Figure 8b profiles 1n–1s for electrokinetic flow) and exchanged concentrations 1 and 2 for the mirror images (Figure 8a profiles 2i-1m for pressure-driven flow and Figure 8b profiles 2n–1s for electrokinetic flow). Subtracting the pressure-driven gradient profiles from the electrokinetic gradient profiles and calculating the standard deviation between the two data sets yields a relative standard deviation between gradients formed with pressure-driven and electrokinetic flows of 0.9%, demonstrating that the gradients generated were very similar.

Our microfluidic device uses a combination of bifurcated and trifurcated channels to form high-quality linear spatial and temporal gradients. Because the number of output steps scales with the number of gradient-forming levels, N, as $2^N + 1$, while the classical pyramidal structures scales as $N + 2$, the entire device is more compact, with linear dimensions smaller by a factor of 10. The compact architecture allows many more gradients per chip for high-throughput applications. The same method also allows us to form gradients with multiple or varying slopes

in a compact footprint. We can also form gradients with complex shapes by appropriately tuning the lengths of the connector channels.

Acknowledgements

We thank Indiana University's College of Arts and Sciences and Biocomplexity Institute for support of this research and Zexi Zhuang and Margaret A. Lerch for assistance with the electroki-netically driven experiments. J.A.G. and D.A. acknowledge support from NSF grant IBN-0083653.

References

1. Dittrich PS, Tachikawa K, Manz A. Anal Chem 2006;78:3887–3907. [PubMed: 16771530]
2. Harrison DJ, Fluri K, Seiler K, Fan Z, Effenhauser CS, Manz A. Science 1993;261:895–897. [PubMed: 17783736]
3. Hadd AG, Raymond DE, Halliwell JW, Jacobson SC, Ramsey JM. Anal Chem 1997;69:3407–3412. [PubMed: 9286159]
4. Kutter JP, Jacobson SC, Matsubara N, Ramsey JM. Anal Chem 1998;70:3291–3297.
5. Kutter JP, Jacobson SC, Ramsey JM. Anal Chem 1997;69:5165–5171.
6. Jacobson SC, McKnight TE, Ramsey JM. Anal Chem 1999;71:4455–4459.
7. Jeon NL, Dertinger SKW, Chiu DT, Choi IS, Stroock AD, Whitesides GM. Langmuir 2000;16:8311–8316.
8. Dertinger SKW, Chiu DT, Jeon NL, Whitesides GM. Anal Chem 2001;73:1240–1246.
9. Lin F, Saadi W, Rhee SW, Wang SJ, Mittal S, Jeon NL. Lab Chip 2004;4:164–167. [PubMed: 15159771]
10. Irimia D, Geba DA, Toner M. Anal Chem 2006;78:3472–3477. [PubMed: 16689552]
11. Wu HK, Huang B, Zare RN. J Am Chem Soc 2006;128:4194–4195. [PubMed: 16568971]
12. Diao JP, Young L, Kim S, Fogarty EA, Heilman SM, Zhou P, Shuler ML, Wu MM, DeLisa MP. Lab Chip 2006;6:381–388. [PubMed: 16511621]
13. Adler J. Science 1966;153:708–716. [PubMed: 4957395]
14. Adler J. J Gen Microbiol 1973;74:77–91. [PubMed: 4632978]
15. Boyden S. J Exp Med 1962;115:453–466. [PubMed: 13872176]
16. Zigmond SH. J Cell Biol 1977;75:606–616. [PubMed: 264125]
17. Zicha D, Dunn GA, Brown A. J Cell Sci 1991;99:769–775. [PubMed: 1770004]
18. Jeon NL, Baskaran H, Dertinger SKW, Whitesides GM, Van de Water L, Toner M. Nat Biotechnol 2002;20:826–830. [PubMed: 12091913]
19. Dertinger SKW, Jiang XY, Li ZY, Murthy VN, Whitesides GM. Proc Natl Acad Sci USA 2002;99:12542–12547. [PubMed: 12237407]
20. Walker GM, Sai JQ, Richmond A, Stremler M, Chung CY, Wikswo JP. Lab Chip 2005;5:611–618. [PubMed: 15915253]
21. Mao HB, Cremer PS, Manson MD. Proc Natl Acad Sci USA 2003;100:5449–5454. [PubMed: 12704234]
22. Koyama S, Amarie D, Soini HA, Novotny MV, Jacobson SC. Anal Chem 2006;78:3354–3359. [PubMed: 16689537]
23. Lin F, Butcher EC. Lab Chip 2006;6:1462–1469. [PubMed: 17066171]
24. Pihl J, Sinclair J, Sahlin E, Karlsson M, Petterson F, Olofsson J, Orwar O. Anal Chem 2005;77:3897–3903. [PubMed: 15987089]
25. Duffy DC, McDonald JC, Schueller OJA, Whitesides GM. Anal Chem 1998;70:4974–4984.
26. McDonald JC, Metallo SJ, Whitesides GM. Anal Chem 2001;73:5645–5650. [PubMed: 11774902]
27. Crank, J. The Mathematics of Diffusion. 2. Clarendon Press; Oxford: 1975.
28. Culbertson CT, Jacobson SC, Ramsey JM. Talanta 2002;56:365–373.

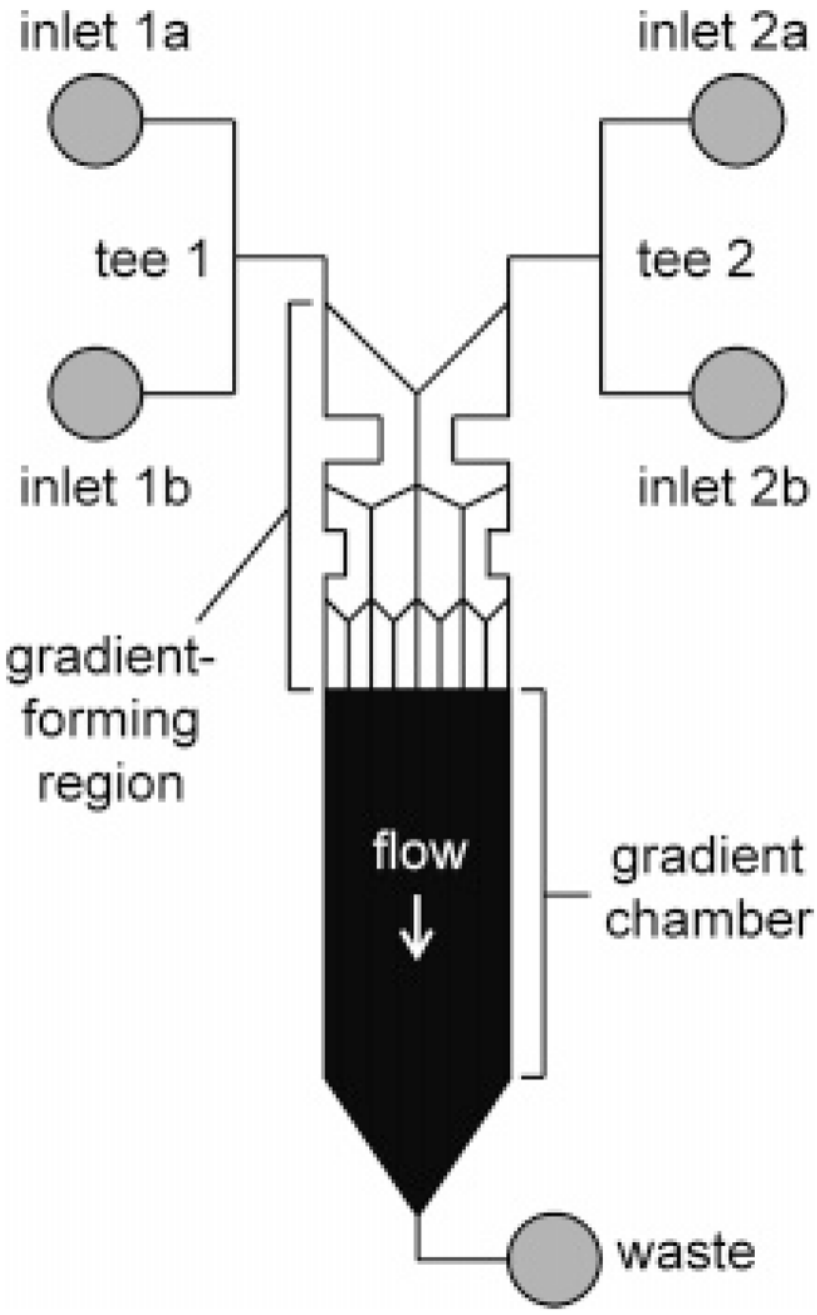

Figure 1.
Schematic of microfluidic device for generating controlled chemical gradients showing the inlets, gradient-forming region, and gradient chamber. Inlets 1 and 2 each have two input reservoirs, denoted a and b. See Table 1 for the parameters and Figure 2 for an enlarged view of the gradient-forming region.

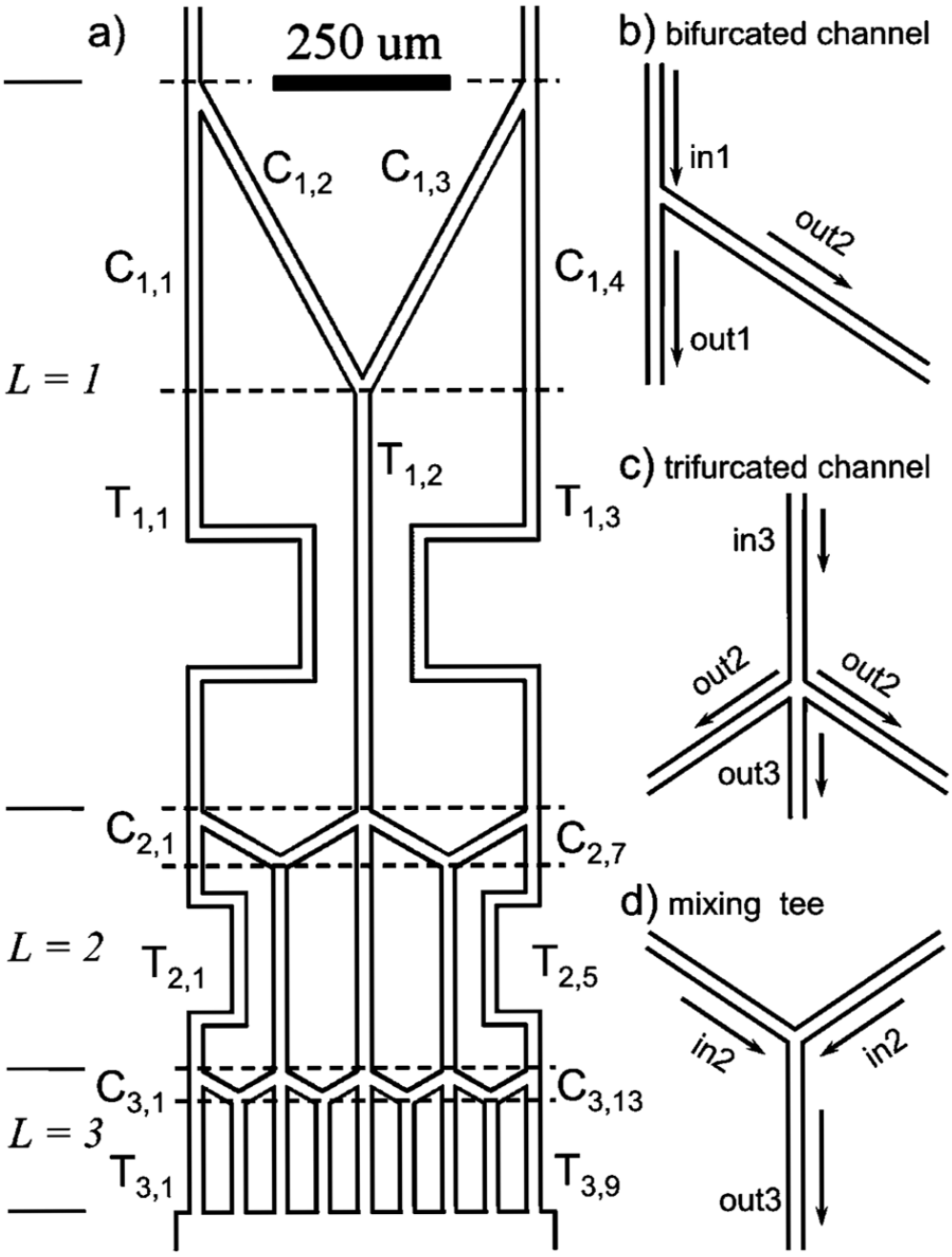

Figure 2.
Schematics of (a) gradient-forming region for device 3-20-60 (see Figure 3a), (b) bifurcated channel, (c) trifurcated channel, and (d) mixing tee. The gradient-forming region has three levels, L = 1–3. The channels have uniform cross section with lengths chosen to balance flow resistance.

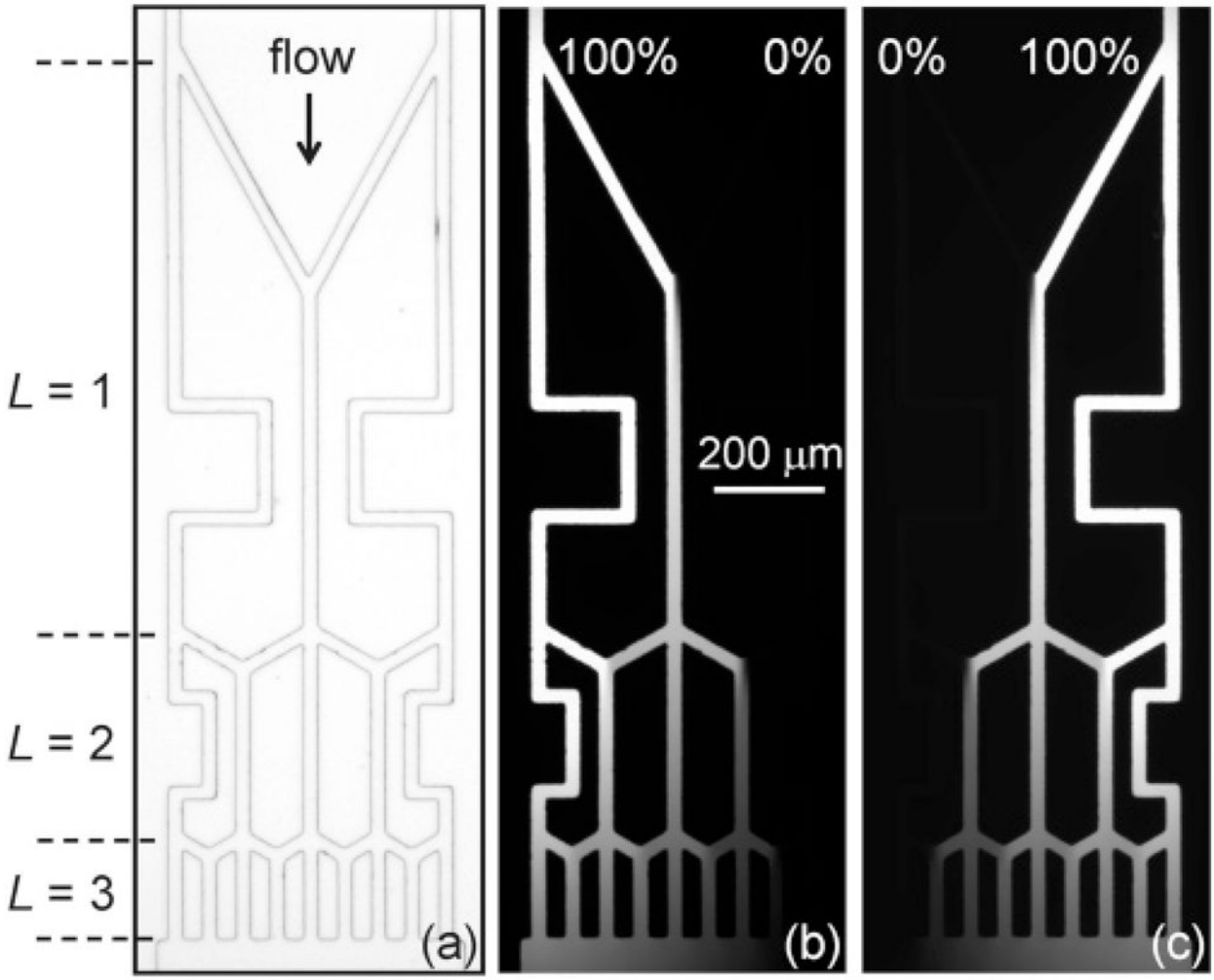

Figure 3.

(a) Transmitted-light image of the gradient-forming region for device 3-20-60 with three levels, 20-μm-wide channels, and 9 output channels with 60-μm center-to-center spacing. Fluorescence images of the gradient for pressure-driven flow with (b) 100% sample at inlet 1 and 0% sample at inlet 2 and (c) 0% sample at inlet 1 and 100% sample at inlet 2. The output channels have concentration steps of 12.5% from 100 to 0% in (b) and 0 to 100% in (c). The scale is the same in all images.

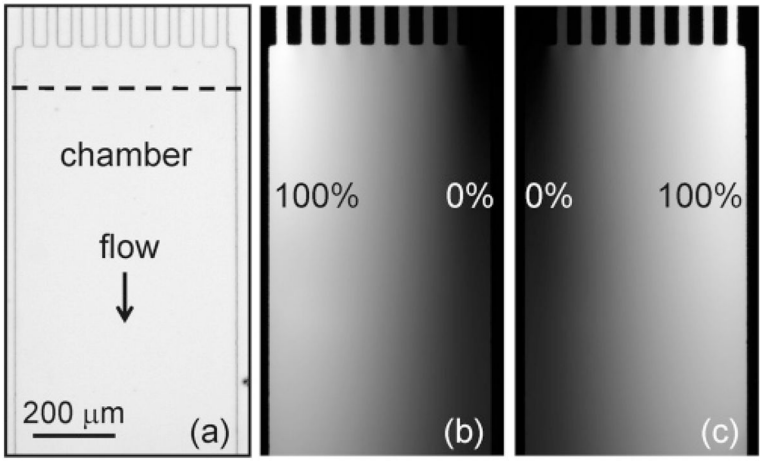

Figure 4.

(a) Transmitted-light image of the gradient chamber for device 3-20-60. The chamber is 540 μm wide. Fluorescence images of the gradient for pressure-driven flow with (b) 100% sample at inlet 1 and 0% sample at inlet 2 and (c) 0% sample at inlet 1 and 100% sample at inlet 2. The inflow to the gradient chamber is in 12.5% increments from 100 to 0% in (b) and 0 to 100% in (c). The dashed line shows the position of the profiles in Figures 5, 6, and 8. The scale is the same in all images.

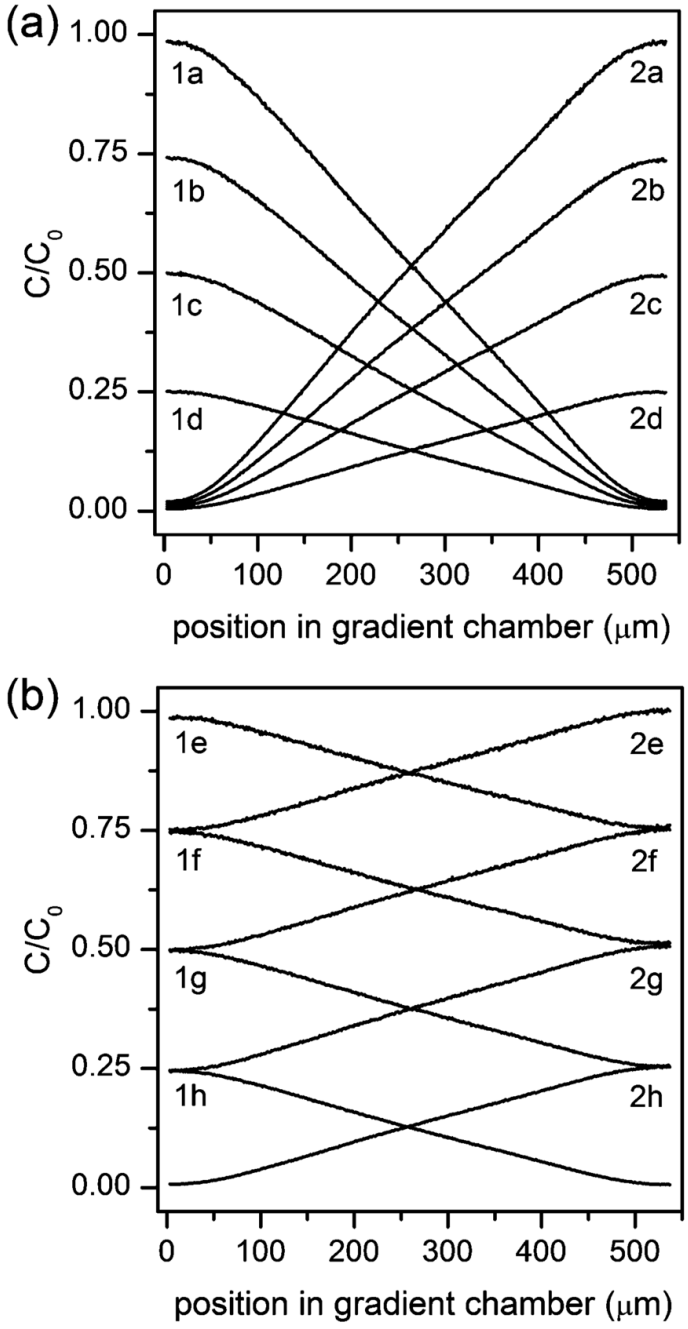

Figure 5.
Gradient profiles (C/C_0) with varying (a) slopes and (b) offsets for device 3-20-60 with pressure-driven flow at $l = 100\ \mu$m along the dashed line shown in Figure 4. Inputs from inlets 1 and 2 correspond to positions in the gradient chamber at 0 and 540 μm, respectively.

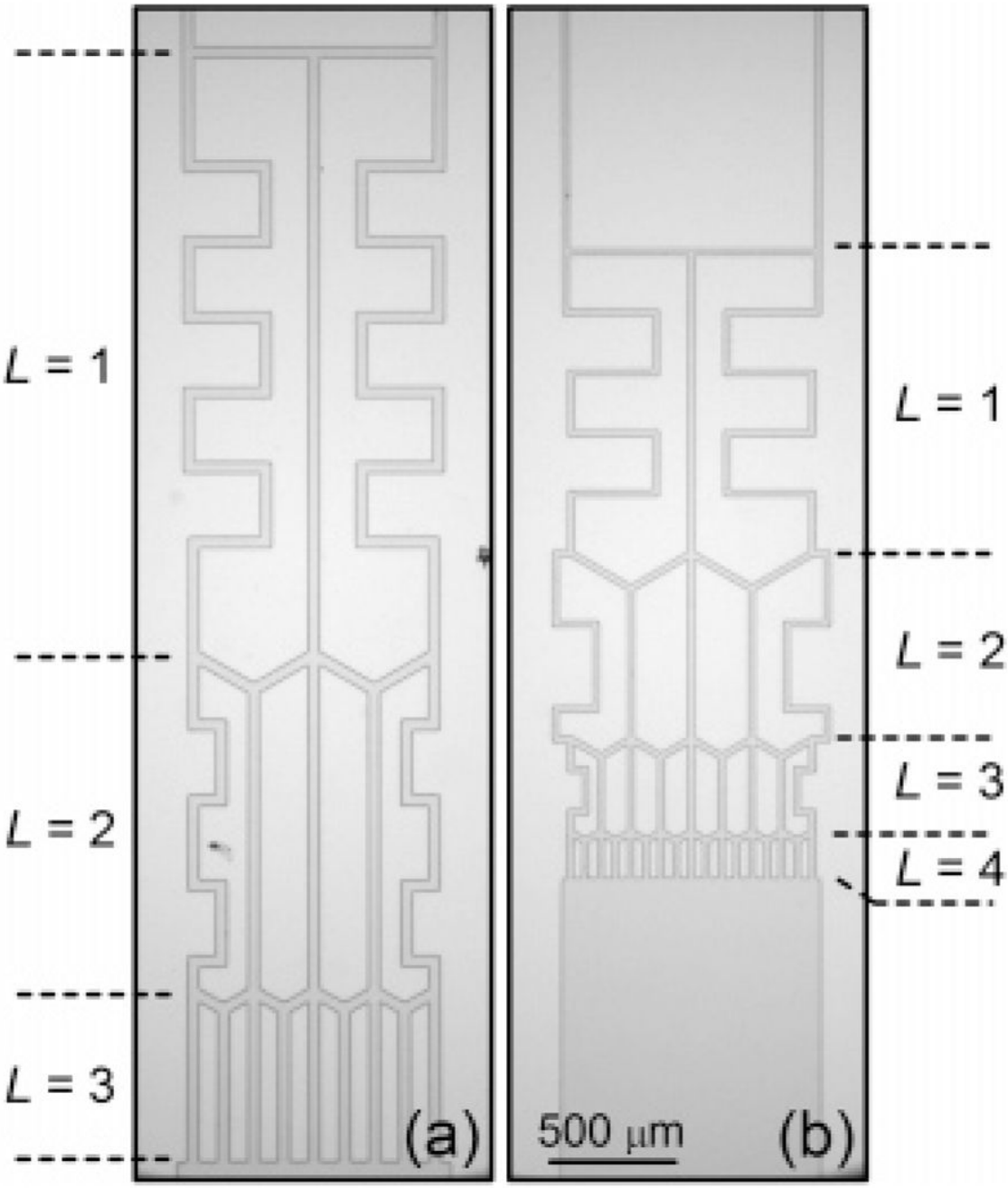

Figure 6.
Transmitted-light images of the gradient-forming region for (a) device 3-40-120 and (b) device 4-20-60. Device 3-40-120 has three levels, 40-μm-wide channels, and 9 output channels with 120-μm center-to-center spacing, and device 4-20-60 has four levels, 20-μm-wide channels, and 17 output channels with 60-μm center-to-center spacing. The scale is the same in both images.

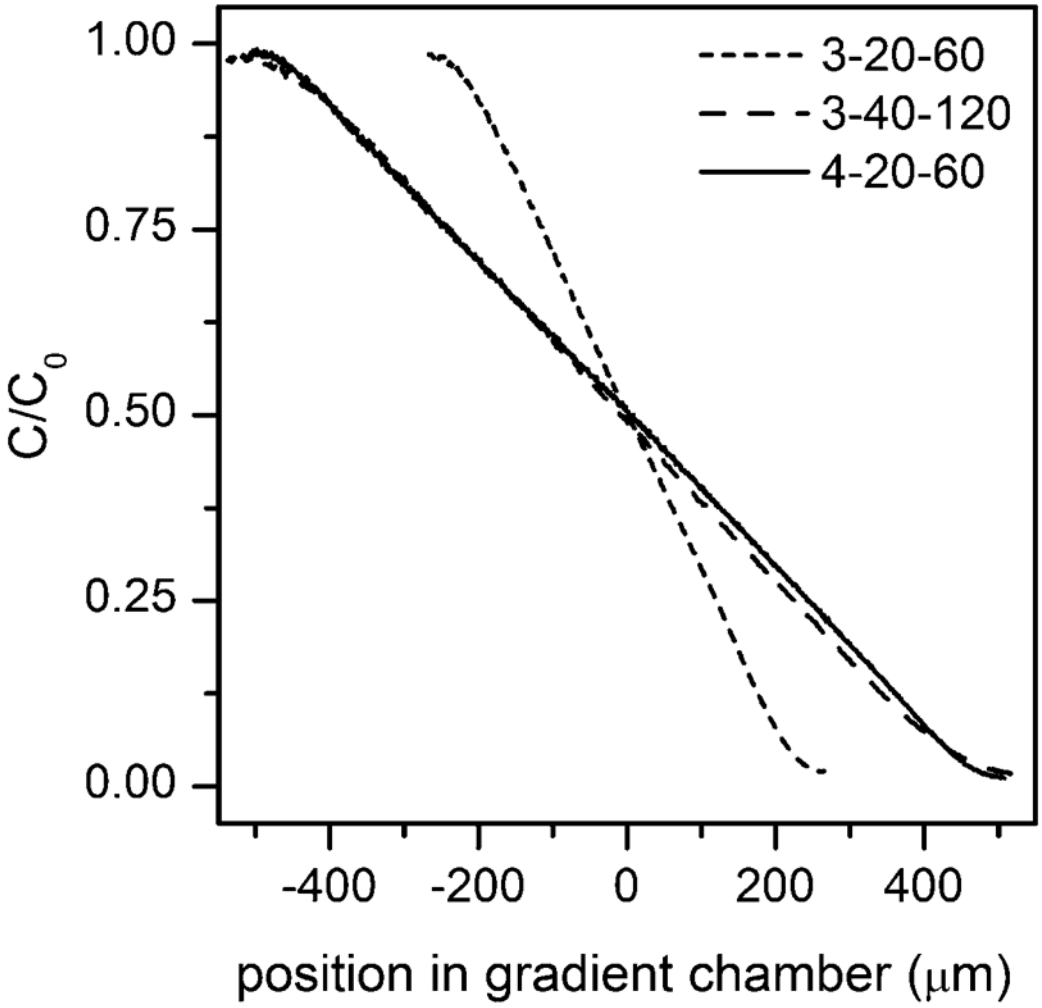

Figure 7.
Gradient profiles for pressure-driven flow generated with devices 3-20-60, 3-40-120, and 4-20-60. See Table 1 for design parameters. The relative concentration of the sample (C/C_0) was measured at l = 100 μm for devices 3-20-60 and 4-20-60 and l = 400 μm for device 3-20-120. Inlet 1 was held at C/C_0 = 1.0, and inlet 2 at C/C_0 = 0. The 0-μm position marks the center of the chamber.

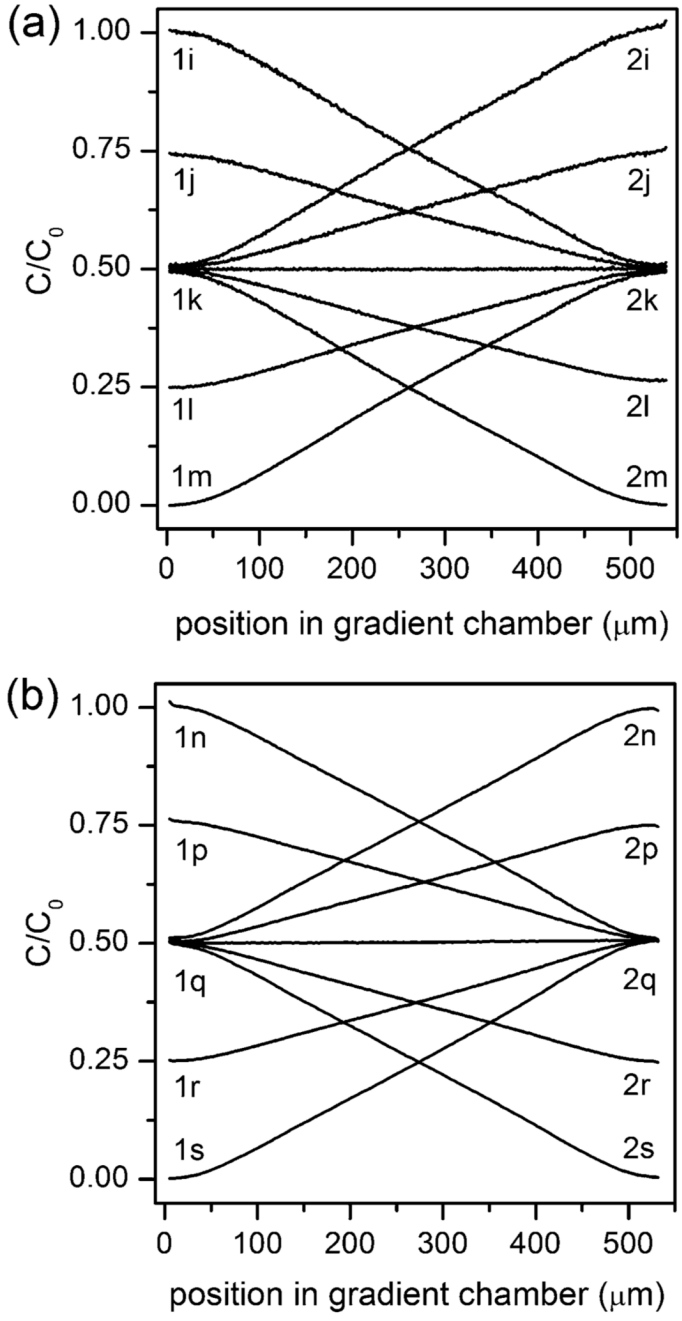

Figure 8.

Gradient profiles at $l = 100\ \mu m$ along the dashed line shown in Figure 4 for device 3-20-60 with (a) pressure-driven and (b) electrokinetic flow. The gradients had a constant offset ($C/C_0 = 0.5$) and varying slopes. Inputs from inlets 1 and 2 correspond to positions in the gradient chamber at 0 and 540 μm, respectively.

Table 1

Microfluidic Gradient-Forming Region Specification

device	no. of levels (*N*)	channel width (*μ*m)	channel spacing[a] (*μ*m)	no. of output channels	chamber width (*μ*m)
3-20-60	3	20	60	9	540
3-40-120	3	40	120	9	1080
4-20-60	4	20	60	17	1020

[a] Center-to-center.